Multi-Resolution Satellite Data Processing for Contextually Relevant Land Use–Land Cover Mapping: Distinguishing Scrublands, Farms, and Plantations Across India

Raman Kumar
ramank.1137@gmail.com
Indian Institute of Technology, Delhi
Delhi, India

Aatif Dar
aatif.dar11@gmail.com
Indian Institute of Technology, Delhi
Delhi, India

Aaditeshwar Seth
aseth@cse.iitd.ac.in.
Indian Institute of Technology, Delhi
Delhi, India

Abstract

Scrublands, vital ecological buffers and livelihood bases for pastoral communities, are increasingly threatened by repurposing initiatives and illegal encroachments. Accurate delineation of scrublands is therefore essential for effective monitoring, resource management, and equitable policymaking. However, existing state-of-the-art (SOTA) global land-cover models, such as Google's Dynamic World, struggle in the Indian context, where rain-fed agricultural fields often exhibit vegetation signatures indistinguishable from those of scrublands. This confusion is further compounded by the absence of high-quality, labeled datasets for these land-use types.

To address these challenges, we developed a computer vision based methodology that leverages high-resolution (1 m) satellite imagery to generate large-scale, high-quality training samples for farms, scrublands, and plantations across India. These samples are used to train improved classifiers that achieve significantly better distinction between farmlands and scrublands than existing SOTA models, while also introducing the first pan-India plantation class. The resulting LULC maps can serve as a reliable foundation for downstream tasks in agroforestry, land restoration, and sustainable resource planning.

ACM Reference Format:
Raman Kumar, Aatif Dar, and Aaditeshwar Seth. 2018. Multi-Resolution Satellite Data Processing for Contextually Relevant Land Use–Land Cover Mapping: Distinguishing Scrublands, Farms, and Plantations Across India. In *Proceedings of Make sure to enter the correct conference title from your rights confirmation email (Conference acronym 'XX)*. ACM, New York, NY, USA, 9 pages. https://doi.org/XXXXXXX.XXXXXXX

1 Introduction

1.1 Background and Motivation

Scrublands play a vital role in India's ecological and socioeconomic fabric. They act as transitional ecosystems between forests and croplands, supporting biodiversity, groundwater recharge, and pastoral livelihoods in semi-arid and dryland regions. For millions of rural and nomadic communities, these landscapes are not wastelands but critical commons that provide fodder, fuelwood, and grazing support and infact these communities have co-evolved with and sustained these ecosystems over centuries.

However, due to its misclassification as wasteland in administrative framework under historical utilitarian logic, these scrublands are often neglected in restorative programs or are prone to degradation, urban encroachments, infrastructure development and tree plantations. This degradation is often overlooked in national land management programs because scrublands are poorly mapped within existing Land Use Land Cover (LULC) datasets.

Accurate delineation of scrublands is thus essential for multiple domains: from ecological restoration and pasture management to climate resilience planning and rural livelihood policy. However, despite growing remote sensing capabilities around the world, the accurate distinction between scrublands, farms, and plantations remains a persistent challenge in mapping efforts in India.

1.2 Problem Definition

The core challenge lies in the spectral and temporal similarity between rain-fed agriculture and natural scrublands. In much of semi-arid India, croplands and scrub vegetation follow similar seasonal greening patterns, both responding to monsoon rainfall. During peak growing periods, spectral indices such as NDVI and EVI show near-identical reflectance trends for both, making it difficult for pixel-based classifiers which are trained on global datasets incapable of icorporating local nuasance which are essential to diffrentiate them.

Plantations are often masked or misclassified as generic "tree cover" or agri-land in most national and global LULC products. This misrepresentation affects not just statistical accuracy but also policy interpretations, for example, when estimating deforestation rates, evaluating afforestation drives or even evaluating true change in cropping intensity.

The lack of high-quality, labeled datasets specifically focused on these three categories—scrubland, farmland, and plantation—has further limited model performance. Without representative samples from diverse agro-ecological zones (AEZs), most classification models either tend to overfit regional characteristics and fail to generalize nationally. State-of-the-art (SOTA) global land-cover datasets, including Google's Dynamic World, ESA WorldCover, WRI and Copernicus Global Land Service, provide valuable global consistency but falter in the Indian context. These models are largely trained on global samples, which do not cover from India's monsoon-dependent and smallholder-dominated landscapes. As a result, they tend to misclassify scrublands as croplands or

Conference acronym 'XX, Woodstock, NY

ACM ISBN 978-1-4503-XXXX-X/2018/06
https://doi.org/XXXXXXX.XXXXXXX

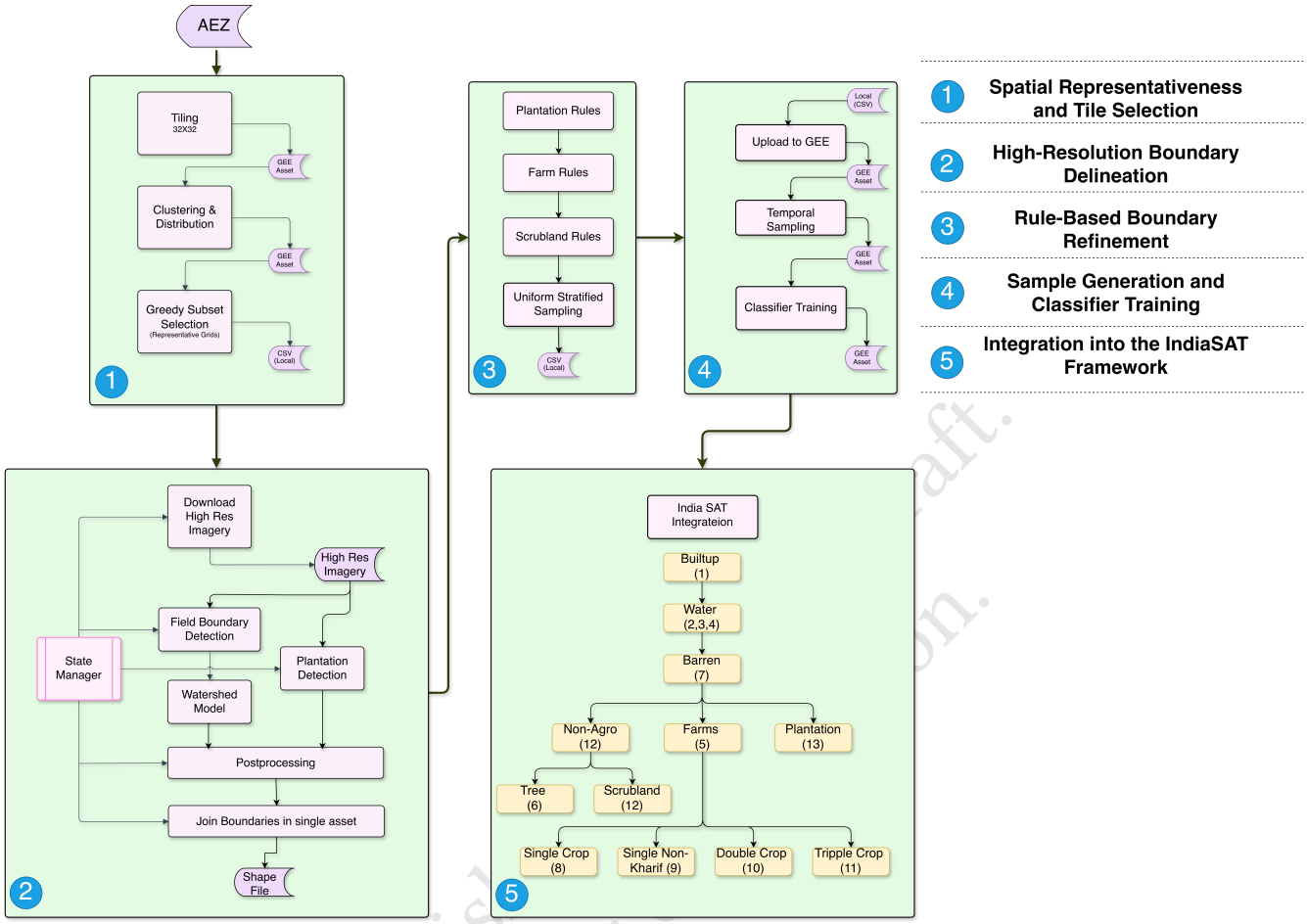

Figure 1: This figure shows the complete pipeline

vice versa, especially in regions with low-input, rain-fed farming systems.

Moreover, many of these products rely on medium-resolution imagery (10–30 m), which lacks the spatial precision to differentiate between mixed or fragmented land parcels—especially smallholder farms and scattered scrub patches that dominate much of the Indian countryside.

1.3 Present Study and Contributions

To address these challenges, we propose a methodology that uses ground truth derived through computer vision methods on hi-res data, as opposed to groundtruth which is normally marked through desk work or field surveys. We presents a viable method to create a large volume of groundtruth from limited hi-res data to train satellite data models that can capture fine-scale spectral, temporal, and morphological nuances which are unique to each agro-ecological zones.

The key contributions of this work are as follows:

(1) **Framework for CV-derived ground truth at scale** We design a generalizable framework that leverages high-resolution imagery and computer-vision pipelines to automatically derive ground-truth labels for distinct land-use types such as scrublands, farms, and plantations. The framework enables the generation of high-quality samples across India without requiring exhaustive manual annotation, providing a scalable and cost-effective alternative for regions that are typically underrepresented due to limited availability of field surveys or desk-based mapping efforts.

(2) **Sampling strategy for selecting hi-res labeling regions**: We propose a sampling method to identify where hi-resolution ground truth should be constructed. By operating on medium-resolution feature embedding clusters and explicitly promoting diversity across all agro-ecological zones, this method yield a set of tiles that are representative and information-rich.

(3) **Hybrid multi-resolution classification framework:** We develop a hybrid classfication approach that integrates hi-resoution samples with medium resolution satelite inputs(google embedding, sentinel2 Landsat Modis) temporal and spectral composites and enables scalable inference at 10m resolution.

(4) **Nationwide plantation layer and pan-India datasets** As an outcome of this methodology, we construct a high-quality, pan-India training dataset for scrublands, farms, and plantations and generate India's first nationwide plantation layer, filling a critical gap in existing LULC products that do not separate plantations from other tree or agricultural classes.

Through these contributions, this study highlights how targeted high-resolution sampling and localized model training can bridge the accuracy gap in global models, paving the way for a new generation of regionally contextualized LULC products.

2 Related Work

TBW

3 Methodology

The framework consists of five sequential modules. It first employs computer-vision techniques on high-resolution imagery to systematically generate ground truth for farms, scrublands, and plantations across India. It maintains geographical and spectral diversity while selecting regions from which high-resolution data are extracted. To scale classification to the national level, a suite of models is then trained using this ground truth along with mid-resolution satellite imagery to produce pan-India inference for these classes. Finally, these outputs are seamlessly merged with other land-cover categories to generate a comprehensive, pan-India Land-Use/Land-Cover (LULC) layer with improved distinction among farms, scrublands, and plantations. The five key components are as follows:

(1) **Spatial Representativeness and Tile Selection** – Identifies spatially and spectrally diverse tiles across agro-ecological zones (AEZs) to ensure balanced geographic coverage and representative sampling.
(2) **High-Resolution Boundary Delineation** – Employs computer vision to delineate high-resolution imagery into various segments which corresponds to farms, non-agro and plantations.
(3) **Rule-Based Boundary Refinement** – Applies a series of geometric, morphological, and contextual rules to eliminate noise and separating out segments corresponding to farm, non-agro and plantations with very high confidence for sample generation.
(4) **Sample Generation and Classifier Training** – Extracts labeled samples from refined boundaries and trains localized classifiers that capture AEZ-specific spectral and temporal characteristics.
(5) **Integration into the IndiaSAT Framework** – Combines AEZ-level outputs into the unified IndiaSAT pipeline, harmonizing classes and ensuring seamless, nationwide scalability.

The detailed methodology for each component is presented in the subsequent subsections. Before running these components, we divide India by using the agro-ecological boundaries that divides India into 20 zones and then run each of the following components for each AEZ. This is done so that we can capture the regional diversity inside a similar looking AEZ.

3.1 Spatial Representativeness and Tile Selection

Our pipeline employs computer-vision techniques on high-resolution imagery (1.19 m at zoom level 17), as small farm holdings are visually distinguishable only at this scale. However, processing imagery at such resolution across the entirety of India is computationally challenging. To address this, we designed a methodology for selecting representative regions that capture the *geographical* and *spectral* diversity across the country.

Let an Agro-Ecological Zone (AEZ) be represented by a set of grids

$$G = \{g_1, g_2, \ldots, g_N\}, \tag{1}$$

where each grid contains 32×32 images of size 256×256 pixels at zoom level 17, corresponding to a 9 km $\times$ 9 km tile. We choose this size as it provides sufficient area for the delineation of farms, scrublands, and plantations in later stages. Each grid g_i is associated with a normalized feature distribution P_i over k clusters obtained using k-means clustering on Google's 64-dimensional embedding vectors computed over the entire G.

To focus on agriculturally relevant regions, urban, water, and barren pixels were masked out using the IndiaSAT LULC layer, restricting sampling to farms, scrublands, and plantations. The goal is then to select a subset

$$S \subset G, \quad |S| = p, \tag{2}$$

such that the aggregated distribution of S,

$$P_S = \frac{1}{|S|} \sum_{g_i \in S} P_i, \tag{3}$$

closely approximates the global AEZ-level distribution,

$$P_{\text{AEZ}} = \frac{1}{N} \sum_{g_i \in G} P_i. \tag{4}$$

This subset-selection formulation enables us to identify a minimal yet representative set of grids for each AEZ, preserving spatial and spectral diversity while keeping downstream high-resolution processing computationally tractable.

Since enumerating all $\binom{N}{p}$ possible subsets is computationally infeasible, we adopt a greedy divergence-minimization strategy. At each iteration, the algorithm selects the grid $g_i \in G \setminus S$ whose inclusion most reduces the Jensen–Shannon (JS) divergence between the aggregated distribution of the selected subset P_S and the global AEZ distribution P_{AEZ}. Formally, the grid added at each step is

$$g^* = \arg\min_{g_i \in G \setminus S} D_{\text{JS}}\big(P_{\text{AEZ}} \,\big\|\, P_{S \cup \{g_i\}}\big), \tag{5}$$

where

$$D_{\text{JS}}(P\|Q) = \frac{1}{2} D_{\text{KL}}(P\|M) + \frac{1}{2} D_{\text{KL}}(Q\|M), \quad M = \frac{1}{2}(P+Q), \tag{6}$$

and D_{KL} denotes the Kullback–Leibler divergence. The process continues until $|S| = p$, typically corresponding to approximately 3% of the total grids per AEZ.

This greedy selection procedure yields a compact yet diverse subset of representative grids whose combined spectral–spatial distribution closely approximates that of the entire AEZ. These grids form the basis for subsequent high-resolution delineation, ensuring that the downstream computer-vision processing reflects

Algorithm 1: Greedy Subset Selection for AEZ Representativeness

Input: Set of grids $G = \{g_1, \ldots, g_N\}$, AEZ distribution P_{AEZ}, desired subset size p
Output: Representative subset S
$S \leftarrow \varnothing$
while $|S| < p$ **do**
  foreach $g_i \in G \setminus S$ **do**
    Compute $D_{\text{JS}}\big(P_{\text{AEZ}} \,\big\|\, P_{S\cup\{g_i\}}\big)$
  $g^* \leftarrow \arg\min_{g_i \in G\setminus S} D_{\text{JS}}\big(P_{\text{AEZ}} \,\big\|\, P_{S\cup\{g_i\}}\big)$
  $S \leftarrow S \cup \{g^*\}$
return S

the full agro-ecological variability across India while maintaining computational efficiency.

Once p grids are selected, each 32×32 grid is further subdivided into four 16×16 grids, which serve as processing units in the on-prem pipeline. The geographic coordinates (top-left and bottom-right latitude–longitude) of each grid are stored in a CSV file to enable consistent downstream processing.

3.2 High-Resolution Boundary Delineation

In this module the high resolution imagery is downloaded at zoom 17 for all the representative grids. Then this module uses computer vision to delineate the high resolution imagery into segments which belongs to farms, scrubland, and plantations. For each segment several geometric and textural features are computed using the RGB image. In the end this module will produce a unified shapefile containing all the shapes of the segments along with their local feature properties. Before starting, each 32 X 32 representative grid is further divided into four 16 X 16 as that is the size which is large enough to give these boundaries and small enough so that the entire pipeline can be executed on a single machine. The geographic coordinates (top-left and bottom-right latitude–longitude) of each grid are stored in a CSV file to enable consistent downstream processing.

3.2.1 Downloading and chunking. We use tms_to_geotiff method from segment-geospatial library which downloads an TMS file and convert it into a geotiff. We download geotiff at zoom 17 for each grid which comprise of 16X16 images each of 256X256 pixels. We further chunk this large geotiff into smaller imager of size 256X256 as the computer vision models runs on this smaller size. These images will pass through two different computervision models. The first model will process these images to produce farms and Non-agricultural boundaries which are further filtered and refined in next module. The second model will process the same set of images to produce plantation boundaries which are again filtered and refined in next module.

3.2.2 Farm and Non-Agricultural Boundary Generation. To delineate farms along with Non-agricultural region we generalized the approach of Wang *et al.*, who trained a FracTAL-ResUNet architecture to delineate agriculture fields on agricultral landscapes. We observed that when we apply their model on mixed landscapes, the model accurately detected farm boundaries where the farms are present. Also, on the scrublands or non-agricultural region, their model creates approximate boundaries. So, we asked the question of whether can we separate these segments into three buckets of farms, scrublands(non-agricultural), and others region (for which we are not sure) based on the local features generated from RGB image for each boundaries. If we can get few sure candidate from each grid of these farms and non-agro region with high confidence, these boundaries can act as ground truth to sample points to train a classifier which can accurately differentiate farms from non-agricultural land.

To extract these boundaries, we ran this model accross all 16×16 grids. We briefly explain the model here. The field-boundary detection backbone follows the FracTAL-ResUNet architecture, which builds on a U-Net encoder–decoder with skip connections and replaces standard residual blocks with FracTAL attention units to enhance feature learning. The network simultaneously predicts field extent, boundary probability, and distance-to-boundary, enabling a multitask formulation that has been shown to improve delineation accuracy. We use the same configuration of depth 6 and 32 filters in the first layer, reported in Waldner et al. for high-resolution field mapping. Since the model outputs boundary probability maps rather than distinct field polygons, we derive individual instances using hierarchical watershed segmentation. The watershed algorithm treats the boundary predictions as a topographic surface and separates fields by "flooding" from local minima until neighboring regions meet at boundary ridges, resulting in closed field polygons. We use the implementation available in the higra package as was used in the original paper. It is to be noted that althogh the FracTAL-ResUNet model ran on an image of 256X256, the watershed algorithm can run on larger area. This answer our question of why we chose the tile which comprise of 16X16 images of 256X256 as this is the largest size that we could compute given our local compute limitation. To run watershed, we first again patch all the 256X256 outputs (boundary probability and field extent) into 16X16 grid and save it and then run our watershed algorithm over this grid output.

Once the segments are generated we compute the geometric and textural feature from RGB images for each boundaries:

- **Entropy** (texture complexity),
- **Rectangularity** (shape regularity),
- **Size** (area).

Entropy was computed using `scikit-learn` mask filters with a disk size of 5. Entropy values > 5.2 for each pixel were summed inside each boundary and an average was taken by dividing it by total number of pixels inside the boundary. Rectangularity was computed as the ratio of segment area to the area of its minimum bounding rectangle (values between 0–1).

These features along with other rules enabled confident labeling of a subset of these boundaries into two broad categories: farms and non-agricultural lands. We call them "easy positives" and they served as the source regions for sampling high-quality training points.

3.2.3 Plantation Boundary Generation. Initial attempts to extract plantations using Hough Transform (based on orthogonal pattern detection) were found inadequate. We therefore fine-tuned a YOLO model trained on manually curated high-resolution plantation

datasets. [PLACE HOLDER (for how the dataset was generated and for training)] A high confidence threshold was enforced to ensure only highly reliable plantation detections were retained. The objective was not exhaustive detection but high-precision extraction of plantation regions to generate trusted samples for subsequent classification.

3.3 Rule-Based Boundaries Refinement

In this module we further refine the boundaries that are obtained in the previous module. From the previous module we get two sets of boundaries, one for farms along with scrublands and another for plantations. Here we first seperate out the high confidence boundaries for farms and scrubland from the first set and then filter the plantation boundaries to remove noise.

3.3.1 Farm and Non-Agricultural boundaries Identification . To get high quality boundaries for farms and scrublands, we used the insight that farms which are man made landscapes will have exhibit less randomness than naturally made scrubland or non-agricultural land. We quantified this randomness using properties like entropy, rectangularity and size. The choice of these properties along with what these properties signifies are discussed below.

Entropy: We quantified local spatial complexity and textural randomness in the imagery by computing per-pixel Shannon entropy using the `entropy` function from the *scikit-image* library [**?**]. For each pixel, entropy was calculated over a disk-shaped neighborhood defined by a morphological structuring element with radius r. Within each neighborhood, the distribution of gray-level intensities was converted into a normalized histogram, p_i, and entropy was computed as:

$$H = -\sum_{i=1}^{L} p_i \log_2(p_i), \tag{7}$$

where L denotes the number of distinct intensity levels in the neighborhood and p_i is the relative frequency of intensity i. The base-2 logarithm yields entropy in bits, with homogeneous regions (low gray-level variability) producing near-zero entropy, while textured or heterogeneous regions yield higher values. The resulting entropy map provides a localized measure of image complexity at the spatial scale defined by the disk radius r. We used r = 5.

Furthermore, to obtain a segment-level measure of spatial complexity, we aggregated local entropy values within each segmented region. We first identified the subset of pixels whose local entropy exceeded a threshold value of 5.2, indicating strongly heterogeneous texture responses. Let $\mathcal{S}$ denote the set of pixels belonging to a given segment and $\mathcal{S}^+ = \{x \in \mathcal{S} \mid H(x) > 5.2\}$ represent the subset with high entropy. The segment-level entropy score is then computed as:

$$\bar{H}_{\mathcal{S}} = \frac{1}{|\mathcal{S}^+|} \sum_{x \in \mathcal{S}^+} H(x), \tag{8}$$

where $H(x)$ is the local entropy value at pixel x and $|\mathcal{S}^+|$ denotes the number of pixels in $\mathcal{S}^+$. This averaging procedure enhances robustness by suppressing the contribution of homogeneous interior regions while emphasizing high-entropy boundaries and structurally diverse areas within the segment.

Rectangularity Measure:

To quantify the shape regularity of each segmented region, we computed a rectangularity score that measures how well the region approximates a rectangle. Let $\mathcal{S}$ be the set of pixels belonging to a segment. We first extract the external contour of $\mathcal{S}$ using the `cv2.findContours` function from OpenCV. The contour area, denoted as A_{contour}, represents the true region area.

Next, we compute the minimum-area rotated bounding rectangle enclosing the contour using OpenCV's `cv2.minAreaRect`, and let its area be A_{rect}. The rectangularity score is defined as:

$$R = \frac{A_{\text{contour}}}{A_{\text{rect}}}, \tag{9}$$

where $R \in [0, 1]$. A value of $R = 1$ indicates that the region is a perfect rectangle, while lower values reflect increasing boundary irregularity due to indentations, curvature, or complex shapes.

Rectangularity was incorporated as a discriminative feature to distinguish between agricultural fields and scrubland regions. Agricultural parcels are typically human-designed, with boundaries shaped by land planning and mechanized cultivation, resulting in near-rectangular forms. In contrast, scrublands exhibit naturally occurring, irregular geometry driven by ecological processes rather than structured land management. Consequently, higher rectangularity scores indicate cultivated farmland, whereas lower scores correspond to scrubland.

Size: We additionally considered the physical size of each segmented region as a discriminative feature. Segment size serves as an important cue for distinguishing agricultural fields from scrublands. Typical farm plots within the study area fall within the range of approximately 500–2000 m^2, based on regional agricultural parcel patterns. In contrast, scrubland regions tend to be considerably larger.

Using the above features we empirically defined rules that gives us few examples of farms and non-agro region in each grid. To obtain farms with high confidence, we found that farms segments usually exhibits an entropy less than 1. This also eliminates farms have high entropy for example plantation. This may also eliminate farms which have high entropy due to scatered trees inside it or gridded cultivation pattern. But since we need only few high confidence farms we can safely ignore them as then will get included by our final model which will be trained on these farms examples. The optimal rectangularity measure that we found which gives farms with high confidence is if the rectangularity value is greater than 0.67. This value gives enough leeway for the irregular farms on the other hand ignoring much of the smaller non-agricultural boundaries. The optimal size for a farm in India that we found out is between 500 to 2000 m2 which comprise of most of the farms sizes in India.

Appart from these values we also found out that when we applied the above rules, we also get isolated boundaries insided non-agricultral areas whoses feature values falls inside the farms filter values. Samples generated from these isolated boundaries becomes noise for training and needs to be eliminated. So it was essential to remove these boundaries. We observed that farms will mostly presents in clusters and rarely present as a single isolated farm which can be safely removed from the set of possible candidates. We removed these boundaries by first generating the farm clusters.

We defined a farm cluster as a cluster of nearby farms whose nearest boundaries are 10 m appart. For each cluster we then compute the number of farms that belongs to that cluster. Then we filter the cluster which have number of farms greater or equlal to three. Eventually we take only those farms which belongs to these clusters of greater than or equal to three.

Therefore, the rules to obtain farms are written as following:

(1) Entropy < 1.0
(2) Rectangularity > 0.67
(3) Size $\in [500, 2000]$ m^2
(4) Boundaries must occur in clusters of three or more to filter isolated noise artifacts

3.3.2 Non-Agricultural area Identification Rules. For scrublands and non-agricultural boundaries, we found out the one rule which works consistently among all the AEZ was the size. The size of these boundaries was consistently large. In general we found out that the size is always greater than 60000 m2. We also kept the upper limit of the size as 5,000,000 m2 to avoid memory overflow when applying the next rule of verifying bigger boundaries against our present LULC.

(1) Size $\in$ [60,000, 5,000,000] m^2, filtering out small intra-farm segments and excessively large regions.
(2) Cross-validation using IndiaSAT v3: boundaries with $> 50\%$ agricultural pixels were excluded to remove false positives (e.g., burnt fields).

3.3.3 Plantation Filtering Rules.

(1) YOLO-derived plantation segments were further filtered by area $\in$ [1,000, 20,000] m^2 to avoid overextended forest regions or scattered tree patches.

3.3.4 Overlap Resolution. Since farm and scrubland boundaries originate from the same model, they are inherently exclusive. However, plantations, which are derived separately, can overlap with either of these. A hierarchical precedence rule was applied:

Plantation > Farm > Scrubland.

This ensured plantations take precedence where overlaps occur, preventing duplicate sampling from the same region.

3.4 Sample Generation and Classifier Training

For each AEZ, high-confidence boundaries from the above steps were used to extract uniformly distributed sample points. Each 16×16 block generated approximately 150 samples per class (farm, non-agro land, plantation), wherever present. Sampling covered roughly 3% of the AEZ's total area. Each sample included geographic coordinates (latitude and longitude) along with the class label, exported to GEE for further processing. This procedure yielded a high-quality, spatially representative sample dataset across India's diverse agro-ecological zones.

To map the entire AEZ at 10 m resolution, we utilized Google's 64-dimensional embeddings, which capture annual summaries derived from multi-sensor satellite data incorporating both spectral and temporal dynamics.

For each sampled point, embedding vectors were extracted for the past three years. This approach assumes that land use remains persistent during this period for the three categories: farms, non-agro land, and plantations. It also offers the added advantage of capturing data for younger plantations; for instance, areas that are full-fledged plantations today may have been young stands three years ago and might not have been detected by our YOLO model but were still included in our samples.

A Random Forest classifier was trained separately for each AEZ using these multi-year embeddings. This AEZ-specific training ensured adaptation to regional conditions and prevented overgeneralization. In this way, a pool of models was created for all AEZs. The resulting models were then used to predict across the entire AEZs, generating a pan India map with three classes; farm, non-agro, and plantation.

3.5 Integration into the IndiaSAT v3 LULC Framework

To create a complete, hierarchical LULC map, the output of our classifier was integrated into the IndiaSAT v3 pipeline as follows:

(1) Initialized background (0) and added built-up (1), water (2), and barren (3) pixels using IndiaSAT v3 modules.
(2) For remaining pixels, applied our classifier output to divide regions into farms, non-agro, and plantations (13).
(3) Further refined:
- Farm regions split into four crop-intensity classes—single Kharif (8), single non-Kharif (9), double (10), triple (11).
- Non-agro regions subdivided using the IndiaSAT tree classifier into forest and non-forest areas; the non-forest areas were designated as scrublands (12).

This multi-stage integration produced India's first scrubland–farm–plantation refined LULC layer, harmonized with existing IndiaSAT class codes.

4 Results

We evaluated the performance of our proposed LULC framework against publicly available reference datasets for different land-use categories. Since no single dataset comprehensively covers scrublands, farms, and plantations, we benchmarked each category against the most relevant open-source datasets as follows:

(1) **Scrublands:** WRI Global Pasture Map Dataset,
(2) **Farms:** AgriField Dataset and 10,000 Fields Dataset,
(3) **Plantations:** Qualitative validation using temporal imagery on Google Earth Pro.

4.1 Evaluation on WRI Global Pasture Map (Scrublands)

The WRI Global Pasture Map provides three categories—(1) Natural/Semi-natural Grassland, (2) Cultivated Grassland, and (3) Other Land Cover. Since our focus is on scrublands adjacent to agricultural areas, only the *Natural/Semi-natural Grassland* class was used for quantitative evaluation. Other classes were excluded due to their mixed composition of croplands, urban, and water features.

Table 1 shows the comparative confusion matrix results for the scrubland class across four datasets: our proposed LULC v4, LULC v3, Google's *Dynamic World*, and ESA *WorldCover* (included here as a placeholder).

Table 1: Comparison of predicted classes for Natural/Semi-natural Grasslands across multiple LULC datasets.

Predicted Class	LULC v4	LULC v3	Dynamic World	ESA WorldCover
Shrub/Scrub	2529	1055	2543	[–]
Tree/Forest	2203	2244	1332	[–]
Barren Land	2058	2058	1216	[–]
Flooded Vegetation	—	—	26	[–]
Grass	—	—	58	[–]
None of the Above	763	2196	2378	[–]
Scruby Sum	6790	5357	5175	[–]
Total Dataset	7553	7553	7553	[–]
Accuracy (%)	89.90	70.93	68.52	[–]

For interpretability, we further derived the conventional accuracy metrics, now extended to include ESA WorldCover (Table 2).

Table 2: Summary statistics for Natural/Semi-natural Grasslands across LULC and global datasets.

Metric	LULC v4	LULC v3	Dynamic World	ESA WorldCover
Natural/Semi-natural Grasslands Detected	5211	[–]	[–]	[–]
Outside Classes 7 and 6	2342	[–]	[–]	[–]
Total Grass Points	7553	7553	7553	[–]
Overall Accuracy (%)	68.99	70.93	68.52	[–]

Interpretation: The proposed LULC v4 model demonstrates a substantial improvement in scrubland detection accuracy over both LULC v3 and global benchmarks. The absolute accuracy gain exceeds 19% compared to *Dynamic World*. The refinement arises from high-resolution boundary extraction and AEZ-specific training that capture regional texture and shape cues overlooked in global models such as ESA *WorldCover* and *Dynamic World*.

4.2 Evaluation on Agricultural Regions

For agricultural regions, we used two independent datasets—the 10,000 Fields Dataset and the AgriField Dataset. Each farm plot was compared against the percentage of farm pixels identified by different LULC products. The results are summarized below.

Table 3: Average accuracy comparison on the 10,000 Fields Dataset.

Model	LULC v3	LULC v4
Farm Pixel Accuracy (%)	80.90	83.08

To facilitate broader benchmarking, Table 5 includes placeholders for additional global LULC datasets (ESA WorldCover, Dynamic World, Copernicus Global Land Service) where similar accuracy metrics will be filled once computed.

Interpretation: The proposed framework consistently outperforms prior LULC versions in delineating agricultural plots, achieving near-perfect correspondence on the AgriField dataset. The improvement is attributed to (i) fine-grained sampling across AEZs, (ii) use of geometric features such as entropy and rectangularity, and (iii) multi-year embedding-based training that stabilizes temporal variations in cropping patterns.

Table 4: Average accuracy comparison on the AgriField Dataset.

Model	LULC v3	LULC v4
Farm Pixel Accuracy (%)	75.66	100.00

Table 5: Placeholder for farm-area accuracy comparison across additional global LULC datasets.

Dataset	LULC v4	LULC v3	ESA WorldCover	Dynamic World
10,000 Fields	83.08	80.90	[–]	[–]
AgriField	100.00	75.66	[–]	[–]

4.3 Qualitative Validation on Plantations

Due to the lack of public plantation boundary datasets, we conducted qualitative validation using temporal imagery on **Google Earth Pro**. We compared the plantation coverage generated by our model from 2017 to 2023 with historical imagery, visually assessing expansion or shrinkage trends across representative regions in Kerala, Tamil Nadu, and Odisha.

The LULC v4 outputs demonstrated consistent detection of plantation patches corresponding to visible canopy expansion in the high-resolution imagery. This longitudinal validation confirms that the model effectively captures gradual plantation growth while maintaining minimal false detections in non-plantation regions. Overall, the results validate that the proposed multi-resolution, AEZ-specific pipeline substantially enhances LULC classification quality across multiple categories, establishing a reliable foundation for downstream applications in agroforestry, ecological monitoring, and land restoration modeling.

5 Discussion

TBW

6 Future Work

TBW

7 Acknowledgments

TBW

Acknowledgments

To Robert, for the bagels and explaining CMYK and color spaces.

References